# Numerical Modeling of Ballistic Impact on Aramid-Reinforced Composite Laminates for Shrapnel Protection

Bui Thanh Phan (buithanh.phan@unob.cz)[1], Michal Petřík (michal.petrik@unob.cz; petrik@vutbr.cz)[1,2], Jindřich Viliš (jindrich.vilis@unob.cz)[1], Bartosz Fikus (bartosz.fikus@wat.edu.pl)[3], Vladimír Horák (vladimir.horak@unob.cz)[1]

[1] University of Defence, Kounicova 65, 662 10 Brno, Czech Republic
[2] Brno University of Technology, Antonínská 548/1, 602 00 Brno, Czech
[3] Military University of Technology, ul. gen. Sylwestra Kaliskiego 2, 00-908 Warsaw 46, Poland

***Abstract*** **- A numerical model was developed to investigate the ballistic resistance of Twaron/epoxy composite laminates subjected to shotgun pellet impact. The modeling framework is based on the finite element method and is implemented within LS-DYNA software. The model enables analysis of impact response behavior and associated damage of the composite laminate. For model validation, ballistic impact experiments and investigations into post-impact damage of the composite laminate were conducted. Experimental pellet penetration depths demonstrated normal distributions of (1.16, 0.09) and (1.19, 0.10) mm. Whereas simulated damage depths across two layers (0.9 mm) and three layers (1.35 mm) matched experimental observations quite well. The developed model offers an effective tool for analyzing the design of fiber-reinforced composite laminates for shrapnel protection, particularly in aerospace and military vehicle applications.**

***Keywords*** **- ballistic impact, fiber-reinforced composites, numerical model.**

## 1. INTRODUCTION

According to statistics and forecasts of the global composite materials market, the adoption of composite materials within the aerospace and automotive sectors has grown significantly and is expected to maintain upward trajectory into the next decade. The aerospace industry has gradually utilized advanced composites in primary structures, while the automotive industry is increasingly leveraging these materials to meet stringent fuel efficiency and emission standards. Both industries demand high strength-to-weight ratios and resistance to corrosion and fatigue in harsh environments [1].

In addition to civil applications, there has been an increasing amount of research and development of lightweight protective systems based on advanced composite materials for military applications. Among these composite materials, fiber-reinforced composite materials, namely carbon, glass, and aramid fiber-reinforced composites, have emerged as leading candidates due to their superior mechanical performance and design flexibility. Compared with conventional metallic materials such as steels and aluminums, they offer high specific strength, high specific stiffness, enhanced corrosion resistance, and improved fatigue properties. In contrast to brittle ceramic materials, their ability to retain structural integrity after multiple impact enhances the long-term survivability of protective systems. Additionally, their structural flexibility allows for the manufacture of complex geometries, reducing assembly steps and production time [2].

Composite materials reinforced with high-performance fibers present a compelling alternative. Their low density combined with high specific mechanical properties enables the design of lightweight and effective armor systems. Weight optimization has been considered as a primary constraint in the design and development of modern ballistic protection systems. In the aerospace sector, where every gram directly affects flight performance and payload capacity, armor systems must be engineered from high-performance, low-density materials to withstand extreme dynamic loads, while meeting long operational ranges. Similarly, for ground armored vehicles, the integration of lightweight protection is essential to enhance mobility, maneuverability, and rapid deployment capability. In combat scenarios, where fuels are often scarce and difficult to transport, weight reduction plays a strategic role in logistical sustainability [3].

The ballistic performance of fiber-reinforced composites is governed by a range of complex damage mechanisms. Energy absorption during impact is primarily associated with dominant fiber failure modes, including tensile rupture and shear plug formation, as well as additional failure modes, including matrix cracking, delamination and fiber-matrix debonding [4], [5], [6]. Although simple analytical models have been proposed to estimate ballistic performance, these approaches are limited to capturing inherent anisotropic behaviors of composite materials. Numerical approaches employed in studies [7], [8], [9] have demonstrated the capacity to reliably simulate the high-velocity impact on various composite materials. By integrating constitutive models that account for anisotropic behaviors of composite materials, these numerical tools allow for accurately modeling the impact response as well as complex damage mechanisms and their evolution under extreme dynamic loading conditions.

For recent decades, there have been various experimental, analytical and numerical studies on ballistics of shotgun projectiles. Earlier studies [10], [11] investigated pellet dispersion based on the Maxwellian distribution. While Deng et al. [12] proposed a numerical model based on finite element method (FEM) and discrete element method (DEM) to simulate interior ballistics of different shotgun projectiles including birdshot and buckshot. Continuing the study on shotgun interior ballistics, Deng et al. [13] developed an extended

numerical model to investigate shotgun exterior ballistics, particularly the pellet swarm flying velocity and the pellet dispersion at various distances from the muzzle. In a study on flight dynamics of spherical pellets, Allen [14] derived analytical formulas for pellet velocity and flight time in free flight. Based on DEM formulations, Zohdi [15] performed simulations of post-impact shotgun pellet ricochet for safety analysis of shotgun blasts. Despite significant efforts made in these studies, there has been limited attention given to shotgun terminal ballistics, especially shotgun pellet impact on composite materials.

The present paper aims to numerically investigate ballistic impact response of Twaron/epoxy composite laminates subjected to shotgun pellet impact. For model validation, ballistic impact experiments were conducted at different shooting distances. By implementing FEM simulations and an advanced computed tomography system, this study provides deeper insights into ballistic impact response of the Twaron/epoxy composite laminates, particularly the depth of penetration. The results obtained in the present work can contribute to the development of reliable predictive models for shrapnel protection.

## 2. EXPERIMENTS

### *A. Composite materials*

Twaron CT 747 fabric, supplied by Teijin Aramid, is a high-performance para-aramid textile. These fabrics are typically designed for applications requiring high resistance to dynamic loading. Basic material properties of Twaron CT 747 fabric, including fabric thickness, areal density, and linear density, are summarized in Table I, as provided by the manufacturer. For the fabrication of the fiber-reinforced composite laminates, woven fabric reinforcements based on Twaron CT 747 para-aramid fibers were employed in conjunction with a polymer matrix system. The matrix consisted of LG700 epoxy resin and HG700 hardener, mixed at a resin-to-hardener weight ratio of 100:30, in accordance with the manufacturer's recommendation to achieve optimal curing and mechanical performance.

TABLE I
Properties of Twaron CT 747 Fabrics [16].

| Fabric | Weave | Thickness (mm) | Areal density (g/m2) | Linear density (dtex) |
|---|---|---|---|---|
| Twaron CT 747 | plain | 0.62 | 410 | 3360 |

Composite laminates reinforced with Twaron CT 747 fabrics were fabricated using the Vacuum Assisted Resin Transfer Molding (VARTM) process in the laboratory of the Department of Mechanical Engineering, Brno University of Technology, Czech Republic. Initially, the dry fabrics were carefully cut into 300 × 300 mm sheets and stacked into layers on top of each other to achieve the desired laminate configuration. The stacked preform was then impregnated by implementing the VARTM process, during which the epoxy resin system was infused under vacuum conditions to ensure thorough wet-out and uniform impregnation of the fabrics. Following resin infusion, the laminates were cured at ambient temperature of 22 °C for a duration of 24 hours, as illustrated in Fig. 1. After complete curing, the fabricated composite laminates consisted of 40 layers with a total thickness of approximately 18 mm, and a measured density of 1280 kg/m³.

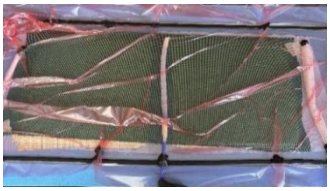


Fig. 1. Curing processes of manufacturing Twaron/epoxy composite laminates.

### *B. Projectiles*

The shrapnel threat was simulated using commercially available shotgun shells provided by Sellier & Bellot manufacturer. Specifically, these shells are loaded with steel pellets, which are spherical in shape with a nominal diameter of 3.05 mm, corresponding to the standard shotgun shot size of US No. 5. The total mass of pellets is 26 g. The shotgun shell and loaded pellets are shown in Fig. 2. According to manufacturer specifications for the selected ammunition type, the muzzle velocity is 360 m/s [17].




(a) (b)

Fig. 2. Shotgun projectile: (a) shell; (b) loaded steel pellets.

### *C. Ballistic tests*

Ballistic tests were conducted to evaluate the ballistic resistance of the Twaron/epoxy composite laminates subjected to shotgun pellet impact. A Baikal over-and-under shotgun, particularly in the classic 16-gauge caliber with a 70 mm chamber and a 740 mm barrel length was used in the ballistic tests. The composite laminate targets were mounted on a rigid support frame at two different distances of 15 and 20 meters from the muzzle. It was assumed that the ballistic tests were carried out at the standard atmospheric condition with negligible wind effects.

The ballistic tests in this study followed earlier ballistic tests involving small-caliber projectiles. Since three previous impacts were localized and substantial undamaged regions remained available for further testing, the same composite laminate was reused for the current ballistic tests and is shown in Fig. 3.



(a) (b)

Fig. 3. Twaron/epoxy composite laminate: (a) before the ballistic tests; (b) after the ballistic tests.

To investigate the influence of shooting distance on pellet penetration behavior, the composite target was divided into two regions. The left half of the target was subjected to pellet impacts at a shooting distance of 20 m, whereas the right half was subjected to pellet impacts at a shooting distance of 15 m. During each test, the half not intended for impact was protected using a shielding plate to ensure that the observed damage patterns were associated with the designated shooting distance. This approach enabled efficient utilization of the composite laminate while preserving the validity and repeatability of the experiments. In addition, a schematic diagram of ballistic tests is illustrated in Fig. 4.

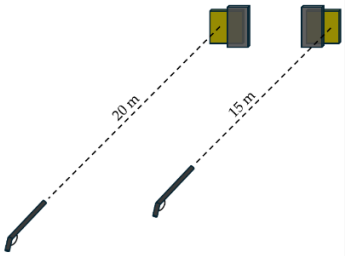



Fig. 4. Schematic diagram of ballistic tests.

## 3. NUMERICAL MODEL

### *A. Assumptions*

In the present study, the impact velocity of the shotgun pellet was determined by theoretical calculations rather than direct measurement. The calculated impact velocity was used as input parameters for subsequent analysis of impact behavior. Although theoretical estimation introduces some uncertainty compared with direct measurement techniques such as high-speed imaging, it provides a reasonable approximation of pellet velocity in practice.

In shotgun pellet dynamics, the radial velocity component of the pellet is much smaller than the axial velocity component. For baseline analysis of pellet penetration behavior, the pellet impact is approximated as normal impact with an impact velocity, which can be determined by a theoretical model with a known muzzle velocity.

Specifically, by assuming that shotgun pellets are not interacting during flight, there are three important forces including air drag, gravity and crosswind force. Among these, the air drag is the major force, whereas gravity and crosswind force are the minor forces. Due to the small mass and high velocity of the pellet, air drag plays a much more significant role in velocity decay over relatively short distances [14]. Therefore, the motion of the pellet can be simply described by the drag equation.

$$m\frac{dV}{dt} = \frac{-1}{2}\rho C_d A V^2 \tag{1}$$

where $m$ is the pellet mass, $\rho$ is the air density, $C_d$ is the drag coefficient, $A$ is the cross-sectional area of the pellet, and $V$ is the instantaneous velocity of the pellet. Note that the drag coefficient $C_d$ for a spherical pellet of diameter $d$ in air can be determined based on the Reynolds number, defined as $\Re = \frac{\rho V_0 d}{\mu}$, where $\rho$ and $\mu$ denote the fluid density and dynamic viscosity, respectively.

For spherical pellets of diameter $d = 3.05$ mm, density $\rho_p = 7850$ kg/m$^3$, and muzzle velocity $V_0 = 360$ m/s, and air of density $\rho = 1.225$ kg/m$^3$ and dynamic viscosity $\mu = 1.8 \times 10^{-5}$ Pa·s, the Reynolds number $\Re$ is about $7.5 \times 10^4$. According to literature [18], for Reynolds numbers in the range of $10^4$ to $10^5$, the drag coefficient $C_d$ is approximately a constant of 0.47.

For the constant drag coefficient $C_d$, integration of Eq. (1) over a distance $s$ yields the velocity $V$ as a function which indicates an exponential decay in pellet velocity with increasing distance $s$ as

$$V(s) = V_0 exp\left(\frac{-\rho C_d A}{2m} s\right) \tag{2}$$

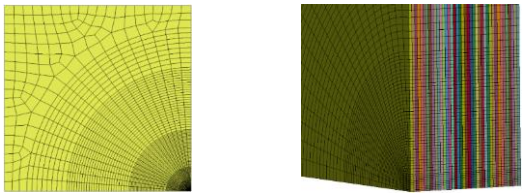
where $V_0$ is the muzzle velocity of the pellet.

As a result, pellet velocities at two distances of 20 and 15 m were determined to be as 280 and 298 m/s respectively.

### *B. Geometry and Mesh*

Numerical simulations of normal impact of the steel pellet on the 18 mm-thick Twaron/epoxy composite laminates were performed using a three-dimensional finite element model within the LS-DYNA software.

Due to the symmetry of geometrical properties, orthotropic material properties and the orientation of the material axes, quarter geometries of the pellet and composite laminate were modeled so that the computation was more efficient. The pellet was meshed by solid elements with an average size of 0.3 mm. The composite laminate of 40 layers was meshed by solid elements with different in-plane sizes. Specifically, each layer was modeled using solid elements with a refined element size of 0.25 mm in the impact zone to resolve localized high-strain gradients, while the far-field region was discretized by a coarser mesh to optimize computational efficiency. In addition, each layer was meshed by one through-the-thickness element with a size of 0.45 mm, which corresponds to the actual layer thickness. The one-fourth geometry and mesh of the composite laminate is shown in Fig. 5.



(a) (b)

Fig. 5. Quarter mesh of the composite laminate: (a) global front view; (b) detailed view through thickness around the impact zone.

### *C. Material models*

Commercial shotgun pellets are typically manufactured from low-carbon steel wire rods. In this study, the pellet material was assumed to be AISI 1006 low-carbon steel. The mechanical behavior of the steel pellet was characterized using the Johnson-Cook constitutive coupled with the Mie-Grüneisen equation of state. The material model parameters for the steel pellet are presented in Table II.

TABLE II
Material Parameters for the Steel Pellet [19], [20].

| Material parameters | | Value |
|---|---|---|
| Density | $\rho$, kg/m$^3$ | 7850 |
| Shear modulus | $G$, GPa | 80 |
| Specific heat capacity | $c_p$, J/kg/K | 452 |
| Strain hardening | $A$, MPa | 350 |
| | $B$, MPa | 275 |
| Strain rate hardening | $n$ | 0.36 |
| | $C$ | 0.022 |
| | $\dot{\varepsilon}_0$, s$^{-1}$ | 1.0 |
| Thermal softening | $m$ | 1.0 |
| | $T_0$, K | 293 |
| | $T_m$, K | 1811 |
| Mie-Grüneisen equation of state coefficients | $C_0$, m/s | 4596 |
| | $S_1$ | 1.49 |
| | $\Gamma_0$ | 2.17 |

The fiber-reinforced composite laminate is considered as an orthotropic elastic material, whose elastic strain-stress relation takes the following form

$$\varepsilon = C\sigma \tag{3}$$

where $\varepsilon$ is the strain vector, $C$ is the orthotropic compliance matrix and $\sigma$ is the stress vector defined as

$$\varepsilon = \begin{bmatrix} \varepsilon_{11} \\ \varepsilon_{22} \\ \varepsilon_{33} \\ \varepsilon_{23} \\ \varepsilon_{31} \\ \varepsilon_{12} \end{bmatrix}, \sigma = \begin{bmatrix} \sigma_{11} \\ \sigma_{22} \\ \sigma_{33} \\ \sigma_{23} \\ \sigma_{31} \\ \sigma_{12} \end{bmatrix}, C$$

$$= \begin{bmatrix} \frac{1}{E_{11}} & \frac{-\nu_{21}}{E_{22}} & \frac{-\nu_{31}}{E_{33}} & 0 & 0 & 0 \\ \frac{-\nu_{12}}{E_{11}} & \frac{1}{E_{22}} & \frac{-\nu_{32}}{E_{33}} & 0 & 0 & 0 \\ \frac{-\nu_{13}}{E_{11}} & \frac{-\nu_{23}}{E_{22}} & \frac{1}{E_{33}} & 0 & 0 & 0 \\ 0 & 0 & 0 & \frac{1}{G_{12}} & 0 & 0 \\ 0 & 0 & 0 & 0 & \frac{1}{G_{23}} & 0 \\ 0 & 0 & 0 & 0 & 0 & \frac{1}{G_{31}} \end{bmatrix}, \tag{4}$$

in which $E$ denotes the Young's modulus, $\nu$ is the Poisson's ratio, and $G$ is the shear modulus. The indices 1,2,3 denote the local material principal axes.

The orthotropic elastic behavior of the fiber-reinforced composite laminate was modeled using the MAT_ENHANCED_COMPOSITE_DAMAGE (MAT_054), which is commonly used in simulations with composites. It assumes a linear elastic orthotropic response of the composite associated with different failure modes including fiber failure in tension, fiber failure in compression and matrix failure.

Material parameters of the orthotropic elastic model for the Twaron/epoxy composite laminate are given in Table III.

TABLE III
Material Parameters for the Twaron/Epoxy Composite Laminate [21], [22].

| Material parameters | | Value |
|---|---|---|
| Density | $\rho$, kg/m$^3$ | 1280 |
| Elastic modulus along the 1-axis | $E_{11}$, GPa | 18.5 |
| Elastic modulus along the 2-axis | $E_{22}$, GPa | 18.5 |
| Elastic modulus along the 3-axis | $E_{33}$, GPa | 6.0 |
| Poisson ratio in the 1-2 plane | $\nu_{21}$ | 0.25 |
| Poisson ratio in the 1-3 plane | $\nu_{31}$ | 0.33 |
| Poisson ratio in the 2-3 plane | $\nu_{32}$ | 0.33 |
| Shear modulus in the 1-2 plane | $G_{12}$, GPa | 0.77 |
| Shear modulus in the 2-3 plane | $G_{23}$, GPa | 5.43 |
| Shear modulus in the 3-1 plane | $G_{31}$, GPa | 5.43 |
| Compressive strength along the 1-axis | $X_c$, GPa | 0.185 |
| Tensile strength along the 1-axis | $X_t$, GPa | 0.555 |
| Compressive strength along the 2-axis | $Y_c$, GPa | 0.185 |
| Tensile strength along the 2-axis | $Y_t$, GPa | 0.555 |
| Shear strength in the 1-2 plane | $S_c$, GPa | 0.077 |
| Compressive strength along the 1-axis | $\rho$, kg/m$^3$ | 1280 |

Delamination between adjacent composite layers was modeled based on a tie-break contact formulation. In this approach, the delamination is initiated once the interfacial stress state, characterized by the normal and shear stresses at the interface, satisfies the following tie-break failure criterion

$$\left(\frac{\sigma_n}{S_n}\right)^2 + \left(\frac{\sigma_s}{S_s}\right)^2 - 1 \geq 0, \tag{3}$$

where $\sigma_n$ and $\sigma_s$ are the normal stress and shear stress in the interface respectively. $S_n$ and $S_s$ are the normal failure stress and shear failure stress in the interface, which are assigned to values of 34.5 MPa and 9 MPa, respectively [21].

## 4. RESULTS AND DISCUSSION

To gain insight into the ballistic impact response of the pellet and Twaron/epoxy composite laminate, the pellet velocity and pellet penetration depth were investigated. Besides the FEM analysis, the pellet penetration depth was specifically analyzed using an advanced micro-computed tomography system.

### *A. Mesh sensitivity analysis*

The mesh density is critical for capturing localized damage in ballistic impacts. Earlier studies [22], [23] of ballistic impact on composite shows that the mesh size ranging from 0.25 to 0.5 mm is sufficiently fine. In this study, a mesh sensitivity study was conducted by refining the element through the thickness of the composite laminate. Two through-thickness mesh sizes including 0.45 and 0.225 mm, corresponding to one and two through-thickness elements in each composite layer, were analyzed. As a result, comparison of penetration depth for both the mesh sizes is illustrated in Table IV.

TABLE IV
Comparison of Penetration Depth for Two Different Through-Thickness Mesh Sizes.

| Impact velocity (m/s) | Penetration depth (mm) | |
|---|---|---|
| | Mesh size of 0.45 mm | Mesh size of 0.225 mm |
| 280 | 1.50 | 1.69 |

The difference in penetration depth is about 10%. To balance accuracy and computational cost, the through-thickness mesh size of 0.45 mm is adopted for further analysis.

*B. Pellet velocity*

Based on the theoretical calculations, the impact velocities of the pellet at the shooting distance of 20 m and 15 m are 280 m/s and 298 m/s respectively. By implementing numerical simulations, pellet velocity histories during impact on the Twaron/epoxy composite laminate at these two impact velocities are derived and shown in Fig. 6. It indicates that the pellet slowed down gradually before temporarily stopping. Notably, the higher impact velocity results in a lower rebound velocity.

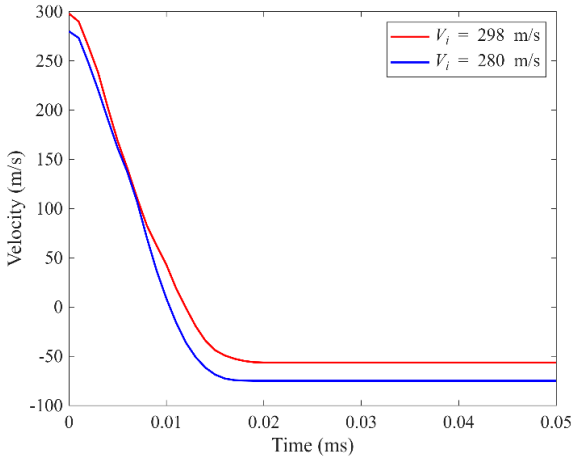
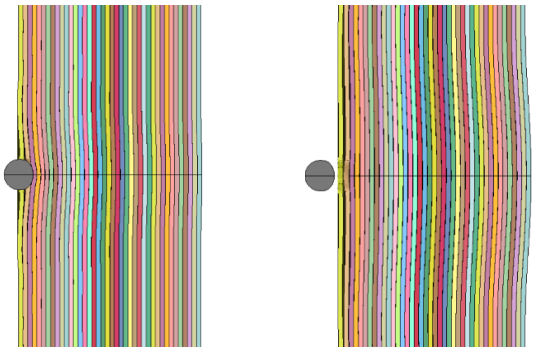



Fig. 6. Pellet velocity histories during impact on the Twaron/epoxy composite laminate.

The decrease in rebound velocity with increasing impact velocity can be attributed to the enhanced energy dissipation and reduced elastic recovery of the damaged aramid-reinforced composite laminate. At relatively lower impact velocities, a greater amount of the deformation can remain recoverable, allowing more stored elastic energy to be released back to the pellet. Whereas, at higher impact velocities, the greater incident kinetic energy causes more irreversible energy dissipation such as fiber rupture, matrix cracking, delamination and friction.

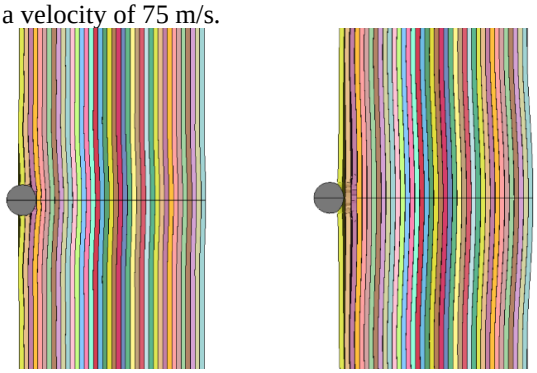
In addition, the approximately linear decay of pellet velocity can arise from the progressive engagement of the relatively thick multilayer composite laminate. For a laminate thickness of 18 mm, corresponding to about six times pellet diameters, the impact response involves sequential layer-by-layer failure. As one layer fails and loses resistance, the pellet immediately engages the next intact layer. During impact, each individual layer undergoes various energy dissipation. Although these individual mechanisms are highly nonlinear, their cumulative effect produces a relatively stable average resistance over the penetration stage.

Simulations of pellet impact on the composite laminate at the impact velocities of 280 m/s and 298 m/s are illustrated in Figs. 7 and 8, respectively. Specifically, these simulations showed that the pellet penetrated first three composite layers and rebounded due to release of elastic energy accumulated within the composite laminate. In addition, the experimental observations revealed that there were partial penetrations and no pellets arrested in the target, which confirms the pellet rebound.



(a) (b)

Fig. 7. Simulation of pellet impact on the composite laminate at the impact velocity of 280 m/s: (a) at 0.010 ms with respect to the penetration depth of 1.50 mm, the pellet temporarily stopped; (b) at 0.040 ms, the pellet rebounded with a velocity of 75 m/s.



(a) (b)

Fig. 8. Simulation of pellet impact on the composite laminate at the impact velocity of 298 m/s: (**a**) at 0.012 ms with respect to the penetration depth of 1.70 mm, the pellet temporarily stopped; (**b**) at 0.040 ms, the pellet rebounded with a velocity of 56 m/s.

*C. Pellet penetration depth*

For quantitative insight into the damage of the Twaron/epoxy composite laminate, the pellet penetration depths were measured and documented by an advanced X-ray micro-computed tomography system, namely the Tescan UniTOM® XL X-ray microtomograph. Particularly, a tomographic cross-section of the impact surface of the composite laminate, which shows the spread of the pellet impact, is represented in Fig. 9.

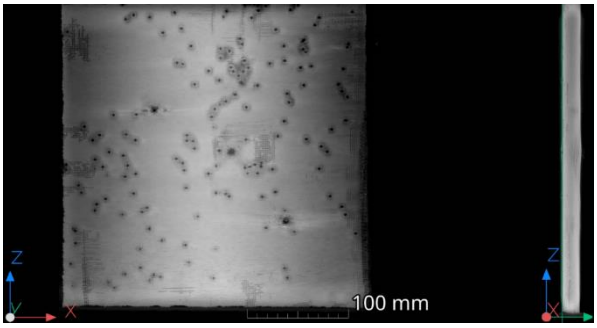
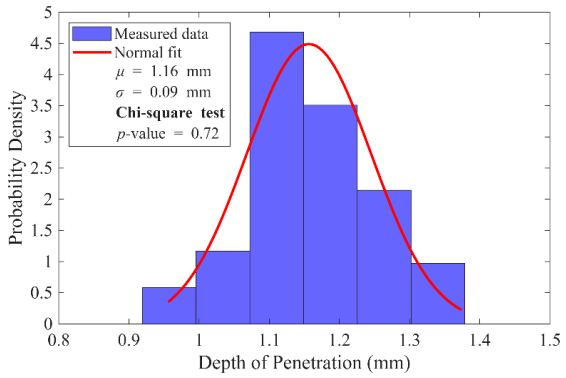


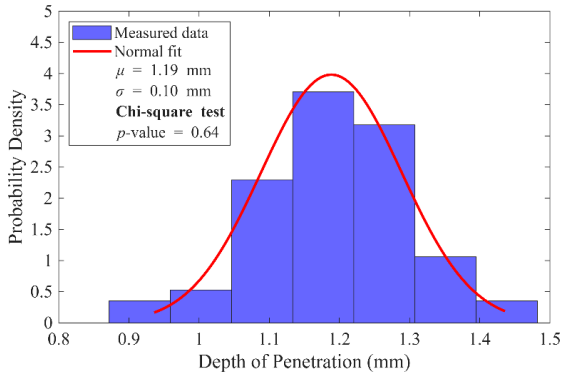

Fig. 9. Tomographic cross-section of the impact surface of the composite laminate.

Probability distributions of the pellet penetration depth in the composite laminate at the shooting ranges of 20 m and 15 m are shown in Fig. 10. These probability distributions are relatively comparable in terms of normal

fitting parameters including means of penetration depth $\mu = 1.16$ and $\mu = 1.19$ mm and the corresponding standard deviation of penetration depth $\sigma = 0.09$ and $\sigma = 0.10$ mm, where the corresponding number of samples $n = 67$ and $n = 65$. In these probability distributions, the number and width of bins were determined based on Scott's rule. Assuming a normal distribution of the measured data, the bin width $h$ was calculated according to this rule as $h = 3.5\,\sigma/\sqrt[3]{n}$, where σ is the standard deviation of the normal distribution estimated from the data and $n$ is the number of samples. Specifically, the bin width $h$ was specified as 0.077 and 0.087 mm respectively. In addition, Chi-square test was used to evaluate how well the dataset fits the normal distribution. The calculated $p$-values of 0.72 and 0.64 demonstrated that the measured data distributions do not significantly differ from the normal distribution.




(a)




(b)

Fig. 10. Probability distributions of pellet penetration depth in the composite laminate at the shooting ranges of (a) 20 m; (b) 15 m.

The numerical simulations showed penetration depths of 1.50 and 1.70 mm, which were larger than those obtained by the experimental measurement. This difference is primarily attributed to the transient dynamic nature of the numerical model, which recorded a maximum penetration depth at the peak of intense elastic oscillations of the composite layers. Whereas the experimental measurement was conducted at the stabilized state where the composite layers experience substantial elastic recovery. Regarding damaged layers, in Figs. 7 and 8 the simulations revealed that the penetration reached two layers (0.9 mm) and three layers (1.35 mm) respectively. This result indicates a reasonable agreement with the experimental observations.

## 5. CONCLUSION

The study proposed a numerical model to analyze ballistic impact response of the Twaron/epoxy composite laminates subjected to shotgun pellet impact. For fundamental analysis of pellet penetration behavior, the pellet impact was assumed as normal impact with an impact velocity, which was calculated based on the aerodynamic drag model. The composite laminate was approximated by an equivalent homogeneous orthotropic material, whose mechanical behaviors were governed by the orthotropic elasticity. Although adopting these assumptions introduced a relatively simplified mathematical formulation of pellet impact on composite laminates, it provided a straightforward and robust approach to simulate the ballistic impact response of the composite laminates for shrapnel protection.

The ballistic impact experiments on the Twaron/epoxy composite laminate were conducted at two different shooting ranges of 20 m and 15 m. At such ranges, the pellet rebound phenomenon was observed in both the simulation and experimental observations. In addition, micro-computed tomography was applied to investigate the post-impact behavior of the composite laminate under ballistic impact of shogun pellets. Particularly, statistical normal distributions $(\mu, \sigma)$ of the pellet penetration depth including $(1.16,0.09)$ and $(1.19,0.10)$ were derived based on the measured data. The simulations yielded higher penetration depths (1.50 and 1.70 mm) than experimental observations due to elastic oscillations of the composite layers. However, the simulated damage depth across two layers (0.9 mm) and three layers (1.35 mm) better correlates with experimental observations.

Acknowledgment

This research was funded by the Ministry of Defence of the Czech Republic "Long Term Organization Development Plan 1011" - Military autonomous and robotic assets of the Faculty of Military Technology, University of Defence, Brno (DZRO-FVT22-VAROPS) and by the Ministry of Education, Youth and Sports of the Czech Republic (Specific Research Project No: SV25-216), and additionally supported by the Military University of Technology under the research project UGB 22-047/2025/WAT (531-000047-W200-22).

## REFERENCES

[1] R. N. Yancey, "Challenges, opportunities, and perspectives on lightweight composite structures: Aerospace versus automotive," in *Lightweight Composite Structures in Transport: Design, Manufacturing, Analysis and Performance*, J. Njuguna, Ed., 1st ed., vol. 67. Cambridge, U.K.: Woodhead Publishing, 2016, pp. 35–52, doi: 10.1016/B978-1-78242-325-6.00002-5.

[2] W. J. Cantwell and J. Morton, "The impact resistance of composite materials—A review," *Composites*, vol. 22, pp. 347-362, 1991, doi: 10.1016/0010-4361(91)90549-V.

[3] R. Zaera, "Ballistic impacts on polymer matrix composites, composite armor, personal armor," in *Impact Engineering of Composite Structures*, S. Abrate, Ed., 1st ed., vol. 526. Vienna, Austria: Springer Vienna, 2011, pp. 305-403, doi: 10.1007/978-3-7091-0523-8.

[4] N. K. Naik and P. Shrirao, "Composite structures under ballistic impact," *Compos. Struct.*, vol. 66, pp. 579-590, 2004, doi: 10.1016/j.compstruct.2004.05.006.

[5] N. K. Naik, P. Shrirao, and B. C. K. Reddy, "Ballistic impact behaviour of woven fabric composites: Formulation," *Int. J. Impact*

*Eng.*, vol. 32, pp. 1521-1552, 2006, doi: 10.1016/j.ijimpeng.2005.01.004.

[6] L. M. Bresciani, A. Manes, and M. Giglio, "An analytical model for ballistic impacts against plain-woven fabrics with a polymeric matrix," *Int. J. Impact Eng.*, vol. 78, pp. 138-149, 2015, doi: 10.1016/j.ijimpeng.2015.01.001.

[7] D. Eckhoff, S. Thomesen, U. Heisserer, and T. Børvik, "Ballistic response behaviour of Dyneema® HB210 curved armour plates: An experimental and numerical study," *Thin-Walled Struct.*, vol. 213, Art. no. 113265, 2025, doi: 10.1016/j.tws.2025.113265.

[8] Z. Zhou, W. Sun, N. Zheng, and L. C. Tang, "Experimental and numerical investigation of the energy absorption characteristics of carbon-basalt hybrid fiber reinforced polymer composites under ballistic impact," *Compos. Struct.*, vol. 335, Art. no. 118000, 2024, doi: 10.1016/j.compstruct.2024.118000.

[9] L. Peng, J. Zhou, Q. Y. Wang, X. F. Zhang, and Z. W. Guan, "Numerical modelling of the ballistic impact response of hybrid composite structures," *Composites Part C: Open Access*, vol. 14, Art. no. 100474, 2024, doi: 10.1016/j.jcomc.2024.100474.

[10] C. Bhattacharyya and P. K. Sengupta, "Shotgun pellet dispersion in a Maxwellian model," *Forensic Sci. Int.*, vol. 41, pp. 205-217, 1989, doi: 10.1016/0379-0738(89)90213-2.

[11] N. K. Nag and P. Sinha, "An investigation into pellet dispersion ballistics," *Forensic Sci. Int.*, vol. 55, pp. 105-130, 1992, doi: 10.1016/0379-0738(92)90118-G.

[12] S. Deng, T. C. Ken, J. Wang, T. C. Wu, and C. C. Lin, "Interior ballistics analysis of shotgun using discrete element method," *Finite Elem. Anal. Des.*, vol. 201, Art. no. 103698, 2022, doi: 10.1016/j.finel.2021.103698.

[13] S. Deng, J. Wang, S. W. Chi, C. C. Lin, J. N. Yeh, and C. C. Lai, "Exterior ballistics analysis of shotgun using discrete element method with equivalent aerodynamic forces," *Finite Elem. Anal. Des.*, vol. 234, Art. no. 104135, 2024, doi: 10.1016/j.finel.2024.104135.

[14] E. J. Allen, "Approximate ballistics formulas for spherical pellets in free flight," *Defence Technol.*, vol. 14, pp. 1-11, 2018, doi: 10.1016/j.dt.2017.11.004.

[15] T. I. Zohdi, "DEM modeling and simulation of post-impact shotgun pellet ricochet for safety analysis," *Math. Mech. Solids*, vol. 26, pp. 1108-1119, 2021, doi: 10.1177/10812865211011217.

[16] Teijin Aramid, "Ballistic materials handbook." [Online]. Available: https://www.teijinaramid.com/en/industries/ballistics/ballistic-materials-handbook. Accessed: Oct. 1, 2018.

[17] Sellier & Bellot, "Non-lead shot cartridges." [Online]. Available: https://www.sellier-bellot.cz/produkty/brokove-naboje/neolovene-broky/detail/5/

[18] S. F. Hoerner, *Fluid-Dynamic Drag: Practical Information on Aerodynamic Drag and Hydrodynamic Resistance*, 2nd ed. Brick Town, NJ, USA, 1965, pp. 37-38.

[19] G. R. Johnson and W. H. Cook, "A constitutive model and data for metals subjected to large strains, high strain rates and high temperatures," in *Proc. 7th Int. Symp. Ballistics*, The Hague, The Netherlands, 1983.

[20] I. A. Bataev, S. Tanaka, A. A. Bataev, K. Hokamoto, V. I. Mali, and M. A. Ribeiro, "Towards better understanding of explosive welding by combination of numerical simulation and experimental study," *Mater. Des.*, vol. 169, Art. no. 107649, 2019, doi: 10.1016/j.matdes.2019.107649.

[21] J. Van Hoof, "Modelling of impact induced delamination in composite materials," Ph.D. dissertation, Carleton Univ., Canada, 1999, doi: 10.22215/etd/2000-04471.

[22] M. R. Millán, C. E. Moreno, M. Marco, C. Santiuste, and H. Miguélez, "Numerical analysis of the ballistic behaviour of Kevlar® composite under impact of double-nosed stepped cylindrical projectiles," *J. Reinf. Plast. Compos.*, vol. 35, pp. 124-137, 2015, doi: 10.1177/0731684415608004.

[23] L. M. Bresciani, A. Manes, A. Ruggiero, G. Iannitti, and M. Giglio, "Experimental tests and numerical modelling of ballistic impacts against Kevlar 29 plain-woven fabrics with an epoxy matrix: Macro-homogeneous and meso-heterogeneous approaches," *Compos. B Eng.*, vol. 88, pp. 114-130, 2016, doi: 10.1016/j.compositesb.2015.10.039.